Renewable Energy 163 (2021) 465–479

Contents lists available at ScienceDirect

Renewable Energy

journal homepage: www.elsevier.com/locate/renene

Energy and exergy analysis of a new solar still composed of parabolic trough collector with built-in solar still

Hossein Amiri [a, *], Mohammad Aminy [b], Marzieh Lotfi [c], Behzad Jafarbeglo [c]

[a] Department of Energy, Institute of Science and High Technology and Environmental Sciences, Graduate University of Advanced Technology, Kerman, P.O. Box:117, 76315, Iran
[b] Materials and Energy Research Center, Karaj, Iran
[c] Graduate University of Advanced Technology, Kerman, Iran

ARTICLE INFO

Article history:
Received 17 February 2020
Received in revised form
18 August 2020
Accepted 1 September 2020
Available online 6 September 2020

Keywords:
New solar still
Parabolic trough collector
Energy
And exergy analysis
Thermal model
Seasons

ABSTRACT

The authors previously proposed and experimentally investigated a new standalone desalination system that is composed of a parabolic trough collector put under conventional solar still. In this study, an unsteady theoretical model is developed using the energy balance equations for the main components of the system to investigate the effect of different parameters on the performance of the new solar still. The model is used for calculation of productivity, and the absorber, saline water, and the glass cover temperatures. Results obtained using the present model are compared with the experimental results and a good agreement is observed between them. Moreover, as the experimental study was limited to the winter period, to thoroughly understand the new system performance at different climates conditions, its performance in four seasons is considered. Results show that in Kerman weather conditions, on average the present solar still system produces 0.961 L of freshwater per day in summer which is 55% more than the yield in winter for the Fixed parabolic trough collector. For the parabolic trough collector with tracking systems, the system would produce 1.266 L per day in summer.

1. Introduction

Freshwater and energy are the most two vital resources in the world. Due to the growth of the human population and increasing living standards, demands for energy and water are increasing steadily, and due to limited resources, they are becoming worldwide challenges to find alternative sustainable resources. Water is a necessity for all living beings, and survival without it is impossible. Providing fresh and healthy water is one of the serious dilemmas in many regions around the globe, especially in dry and secluded areas. Desalination is a process that removes salt, pollution, and other mineral components from saline water, and convert it to a useful form. Desalination is an energy-consuming process.

Energy is the key to economic and social development. However, the use of traditional fossil fuel energy sources has adverse environmental effects. Solar energy is abundant, clean, plentiful, and renewable energy. This energy is considered as one of the most promising alternatives for fossil fuels. Solar stills are cheap, simple to construct, have a low maintenance cost, and does not require fossil fuels. Therefore, they are considered as a suitable solution for places that have limited freshwater resources. However, the low efficiency and low production rate of standard solar stills offset their advantages.

Various parameters, design conditions, and modifications that affect the performance and productivity of solar stills were investigated by several researchers [1–7]. These factors can be loosely classified into three main categories i.e. meteorological and geographical factors, design parameters, and operational parameters [8]. Meteorological and geographical factors are solar radiation hitting the ground, ambient temperature, latitude angle, wind velocity and humidity, sky clearness, etc. Design parameters include absorber properties and its orientation, condenser properties and its orientation, insulation properties, solar intensity on the absorber, the free surface area of saline water, and cavity aspect ratio. Operational parameters include feed water temperature and its flow rate, basin water depth, location, slope, the orientation of

* Corresponding author.
E-mail addresses: hosseinamiri2010@gmail.com, h.amiri@kgut.ac.ir (H. Amiri).

https://doi.org/10.1016/j.renene.2020.09.007
0960-1481/

still. Even though the solar still output can be significantly affected by meteorological and geographical features, however, they are out of human control. Recently, Arunkumar et al. [2] reviewed and categorized the different solar still designs with high productivity and discussed their novel modifications.

The water-to-glass temperature difference is one of the main parameters affecting the freshwater production of standard solar stills. Design parameters and operational parameters affect water-to-glass temperature. Increasing in temperature difference between water and the glass cover can be attained either by increasing the basin water temperature using active or passive methods or by decreasing the glass cover temperature or a combination of them [9–11]. Somwanshi and Tiwari [9] showed that the flow of water from an air cooler over the cover of single basin solar still can increase the annual yield of still up to 56.5%. Zaki et al. [12] experimentally compared the performance of a simple still and a similar still coupled to an external trough type concentrator. Due to an increase in the glass to cover temperature, the productivity of the assisted still was 22% higher than that of the simple still. Aburideh et al. [13] investigated the effect of operating parameters of the double slope solar still on its performance. They found that productivity increases when the difference between the temperature of water and glass covers increases.

One of the techniques to improve the productivity of solar still is the combination of solar still with other devices such as reflector, solar collector, and concentrator [4,14]. Many researchers used concentrator technology to increase the productivity of solar desalination systems. The productivity of modified stepped solar still with internal reflectors is experimentally investigated by Omara et al. [15]. They showed that using internal reflectors in the stepped solar still can increase its productivity up to about 75% higher than that for a standard solar still. Tanaka [16] designed and experimentally investigated a solar still with internal and external reflectors. He found that using reflectors in solar still could increase daily yield by 70–100% on winter days. Omara et al. [17] investigated the effect of internal and external reflectors on the stepped solar still. Their experimental results indicated that the modified stepped solar still with internal and external reflectors have approximately 125% higher yield than the standard solar still. Tiwari and Suneja [18] proposed an inverted reflector solar still and numerically analyzed it.

To improve the productivity of the solar still, a combination of various types of concentrators with solar still have been proposed and studied in the past. Chaochi et al. [19] proposed a solar desalination unit equipped with a parabolic concentrator. They developed a theoretical model to evaluate the absorber temperature along with the distillate flow rate as a function of solar radiation. Results show that the flow rate obtained using the theoretical model had an average relative error of 42%. Gorjian et al. [20] designed, fabricated, and experimentally evaluated a stand-alone point-focus parabolic solar still for seawater desalination. Results show that the maximum daily yield and efficiency of the solar still was 5.12 kg/m2/day and 36.7%, respectively.

Different couplings of solar still with other solar collectors have been proposed [21]. Arunkumar et al. [22] fabricated and experimentally evaluated the performance of four non-concentrating solar still and three concentrating solar stills. Their results showed that the pyramid solar still coupled with compound parabolic collector had maximum productivity. Malaeb et al. [23] considered adding slowly rotating drum within the still that leads to the formation of thin water films over the drum and increase water evaporation.

Thermal analysis or modeling, i.e. energy and exergy modeling, is a powerful tool for design, evaluation, and optimization of thermal systems. Sharshir et al. [24] reviewed the theoretical approaches including energy and exergy analyses which have been used to evaluate the thermal performance of active and passive solar stills. They had concluded that the present designs of solar stills are incomplete and need further improvements. Kianifar et al. [25] built, tested and performed energy and exergy analysis of two pyramid-shaped solar still with/without a small fan. The results showed that during summer, solar still with the fan has higher exergy efficiency than the one without the fan, while in the winter both solar stills have pretty much the same exergy efficiency.

Although many pieces of research have been conducted to enhance the efficiency of solar stills, it seems that there is still a gap between the best design for the solar still (which produce water at low cost and optimal rates) and its present design. Thus, every year several methods and plans are presented to improve the efficiency of solar stills. The literature review shows that little attention has been devoted to the development of stand-alone solar desalination units that employ parabolic trough concentrators/collectors. Desalination of brackish water employing parabolic trough collector makes it possible to reach higher temperatures for the saltwater (brackish or saline water) in the solar still that leads to an increase in evaporation rates. Recently, Amiri et al. [26] proposed a new and innovative stand-alone desalination system. In this system, a solar still is integrated into a parabolic trough collector. The new design improves the standard solar still design while keeping the simplicity of standard design. This standalone system is cheap and has low maintenance costs which have potential on increasing productivity and can be used in rural and coastal areas without any problem. The present work is an attempt to theoretically modeling the new solar desalination system proposed by Amiri et al. [26]. In this study, a thermal model (zero-dimensional thermodynamic model) is developed for the new solar desalination system. This model will be used to predict the transient energy and exergy performance of the device and its component in different conditions. To reduce the cost and complexity of the new desalination system, in the experimental work [26], the design was so that the parabolic trough collector does not track the sun. In the present work, the performance of new solar still with a parabolic collector that follows the sun, i.e. using a tracker for the parabolic collector, will be evaluated numerically, and compared with the fixed collector. Another goal of this study is to evaluate the performance of the new solar system across the entire seasons of a year to understand the system performance at different weather conditions.

2. Review of experimental set-up and procedure

Fig. 1 shows the proposed solar desalination system consists of a parabolic trough collector used as reflector and concentrator of the solar radiation and a solar still. A pictorial view of the new solar still integrated into a parabolic trough is shown in Fig. 1a, whereas Fig. 1b is a schematic of the new desalination system.

The solar still is positioned at a focal point of the parabolic trough collector. The solar still has 60 cm long, 10 cm wide and 38 cm of height. The still was fabricated using a Plexiglas sheet. The condenser surface of the still was also made of Plexiglas. Eight stainless-steel sheets with 60 cm long and 20 cm wide were added to the top of the still to increase the condensation rate. As the Plexiglas is effectively transparent to solar radiation, a stainless-steel sheet of 1.5 mm thickness coated with non-reflective black paint with 60 cm long and 25 cm wide was used as an absorber that furnishes the bottom and two sides of the still up to 7.5 cm. The saline water depth in the basin was kept constant (4 cm) by using a float valve. Also, a 5 cm air gap has been devised under the absorber to reduce heat loss from the absorber of the solar still to the ambient. To keep the desalination system simple, the concentration ratio is designed to be below 10. Thus, the parabolic collector can be

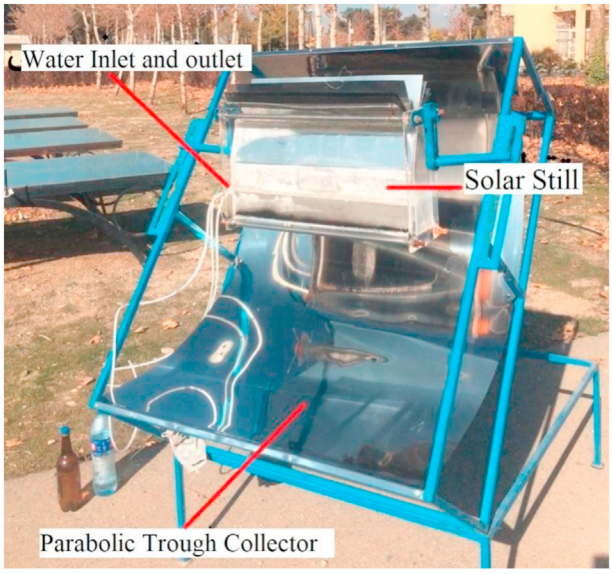

a)

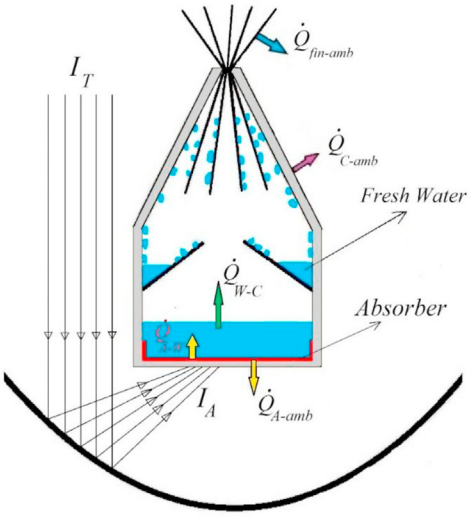

b)

Fig. 1. a) a photograph of the new solar still [26], b) schematic diagram of the new solar still and heat transfer flowchart.

- The temperature of the absorber, brine water, and the cover glass are assumed uniform over their domains, but they are time-dependent. Even though the solar radiation reaches to the back of the absorber may not be uniformly distributed over the absorber (considering that the parabolic trough collector is a one-axis concentrator) especially in the morning and afternoon, but as the thermal conductivity of steel used as the absorber is relatively high and the absorber covers some part of side walls, a rough estimation could prove that the temperature distribution is relatively uniform over the absorber. Moreover, as solar radiation is low in the early morning and late evening, it has a low impact on the performance of solar still and this assumption is more justified.
- As the one-day performance of solar still is considered in this study, it is assumed that the drainage water leaves the still at the end of each day. Therefore, the effect of energy and exergy leaving the still with brackish water is not considered here.

used without a tracking system. However, the parabolic trough collector is mounted on an adjustable-slope steel frame that rotates about the horizontal east-west axis. The slope of the collector was adjusted at the monthly optimal slope angle proposed by Jafari and Javaran [27].

The experimental setup was installed at the Graduate University of Advanced Technology (30.06° N and 57.29° E), Kerman, Iran. The proposed system was tested in Dec 2015, and Jan 2016. The saline water temperature and absorber temperature were measured at intervals of 15 min. The absorber temperature was measured at the center of the absorber and the water temperature was measured at 2 cm above the center of the absorber, i.e., the midpoint of the water depth. Thermocouples with an accuracy of ±1 °C, connected to a multi-channel digital data logger were used to measure the temperatures of the absorber and water. Kipp & Zonen CM6B pyranometer with an accuracy of ±10 W/m^2 was used to measure the intensity of incident solar radiation on the ground. The distilled output of solar still was measured by a calibrated flask with an accuracy of ±10 mL (±0.01 L) at regular intervals of 1 h.

3. Mathematical model

The thermal model is developed by the application of energy conservation equation for each component of solar still separately. The main energy transport mechanisms in the still are shown in Fig. 1b. To simplify the governing equations following assumptions have been made:

- The inclination of the glass cover is not considered. But in evaluating the area of the glass cover, its inclination angle is considered.
- The system is in a quasi-steady state condition.
- As all the gap was covered with silicone sealant in the experiment, it is assumed that there is no water and vapor leakage from the still.
- The physical properties of the absorber, water, and the glass cover are assumed constant in the operating temperature range and are taken equal to their values at mean temperature.

In what follows, energy and exergy analysis for different components of a solar still will be presented.

3.1. Energy analysis

3.1.1. Absorber

Application of the energy conservation equation to the absorber plated gives the following equation:

$$m_A c_{p,A} \frac{dT_A}{dt} = \dot{Q}_{sun-A} - \dot{Q}_{A-W} - \dot{Q}_{A-amb} \quad (1)$$

where, $\dot{Q}_{sun-A} = I_A A_A$ is the rate of solar energy reached to the back of absorber; A_A, m_A, $c_{p,A}$ and T_A are area, mass, specific heat, and temperature of the absorber plate, respectively; $\dot{Q}_{A-W}$ is the rate of convection heat transfer from the absorber to water; $\dot{Q}_{A-amb}$ is the rate of heat loss from the absorber to ambient (heat loss through the bottom of the solar still); t is time, and $I_A$is concentrated solar irradiance hits the bottom of the absorber and is obtained from the following equation:

$$I_A = \alpha \times \tau_{g1} \times \tau_{g2} \times r \times CR \times I_T \quad (2)$$

where, α, τ, r, $CR = A_{Ap}/A_A$ and I_T are solar absorption of the absorber, the transmittance of the Plexiglas, solar reflectivity of stainless steel used in the parabolic trough collector, area concentration ratio of the collector, and solar irradiance hitting the aperture of the collector, respectively. Subscribe $g1$and $g2$stand for two layers of the Plexiglas at the bottom of the solar still. In this study, the area concentration ratio is $CR = 6.4$. As in this study, CR is less

than 10, the effective incident radiation measured on the plane of the aperture $I_T$includes beam and diffuse radiation in contrary to the high concentration cases where diffuse radiation is neglected [28].

Solar irradiance over the aperture area, I_T, is obtained using the isotropic sky model with the ground albedo of 0.2 [28]. In the experiment, the slope of the aperture surface of the parabolic trough collector was monthly adjusted to the optimal slope proposed by Jafari et al. [27]. For this condition, incidence radiation is modified to account for deviations from the normal of the angle of incidence of the radiation on the aperture, as follows [28]:

$$I_T(Fixed@\beta) = I_{T,iso}(\beta)\cos(\theta) \tag{3}$$

where $I_{T,iso}(\beta)$ is solar radiation over a sloped surface facing south with a sloped angle of β; θ is the angle of incidence of solar radiation over the aperture. Other losses including incidence angle modifier are ignored.

A numerical study is performed to evaluate the performance of the new system if a one-axis tracking system rotating about a horizontal east-west axis with the continuous adjustment is implemented in the parabolic trough collector. In such condition, solar radiation over the collector is obtained using the following equation:

$$I_T(Track) = I_{T,iso}(Track) \tag{4}$$

where $I_{T,iso}(Track)$is solar irradiance over the aperture when parabolic trough collector tracks the sun. The angle of the incident and the slope of the aperture of the parabolic collector for the tracking condition is given in Ref. [28].

In Equation (1), convection heat transfer from the absorber to water, $\dot{Q}_{A-W}$, is calculated from the following equations:

$$\dot{Q}_{A-W} = h_{c,A-W}A_A(T_A - T_W) \tag{5}$$

where, $h_{c,A-W}$ is the convective heat transfer coefficient between absorber and water and is calculated from Ref. [29]:

$$h_{c,A-W} = C\frac{k_W}{X_W}(Gr\Pr)^n \tag{6}$$

where, $C = 0.54$ and $n = 0.25$ if $Gr\Pr < 10^7$, otherwise $C = 0.15$ and $n = \frac{1}{3}$. In the above equation,k_W is water thermal conductivity; X_W is the characteristic length of water; Gr and Pr are Grashof and Prandtl numbers, respectively.

Heat loss from the absorber to ambient is calculated by

$$\dot{Q}_{A-amb} = UA_A(T_A - T_{amb}) \tag{7}$$

where T_{amb} is ambient temperature and U is overall heat transfer coefficient for heat transfer from the basin (absorber) to the ambient and is obtained from:

$$U = \left[\frac{k_P}{L_P} + 2\frac{k_P}{L_P} + \frac{1}{h_{c-\infty}}\right]^{-1} \tag{8}$$

where, k_P and L_P are thermal conductivity and thickness of Plexiglas sheet (in the above equation "2" stands for two layers), respectively; k_{air} and L_{air} are thermal conductivity and the air gap length, respectively; $h_{c-\infty}$ is the convective heat transfer coefficient between the bottom surface of the absorber and the ambient air, and is calculated using [29]:

$$h_{c-\infty} = \left(k_{air} \Big/ L_{bot} \times 0.27(Gr\Pr)^{0.25}\right) + 3.8V_w \tag{9}$$

where L_{bot} is the characteristic length of the bottom surface of the still and $V_w$is the wind speed. Since wind speed was low in the experiment, therefore $V_w = 0.0$.

3.1.2. 3-1-2- Brackish water

Conservation of energy for the brackish water is as follows:

$$m_W c_{p,W}\frac{dT_W}{dt} = \dot{Q}_{A-W} - \dot{Q}_{W-C} + \dot{m}_{in}c_{p,W}T_{in} - \dot{m}_{dw}c_{p,W}T_W \tag{10}$$

where, $m_W$and $c_{p,W}$ are mass and specific heat of the water in the still, respectively; $\dot{m}_{in}$, $\dot{m}_{dw}$, and T_{in} are brackish water input rate, freshwater (distilled water) production rate, and temperature of input brackish water. It is assumed that the brackish drainage water drains at the end of the experiment. Thus, to keep the water depth in the still constant $\dot{m}_{in}$ must be equal to $\dot{m}_{dw}$, i.e. $\dot{m}_{in} = \dot{m}_{dw}$. Furthermore, it is assumed that the temperature of input brackish water is equal to average ambient temperature through the whole year ($T_{in} = 18\ ^0C$). $\dot{Q}_{W-C}$ is overall heat transfer between water and cover (condenser) and is evaluated from the following equation:

$$\dot{Q}_{W-C} = h_{W-C}A_C(T_W - T_C) \tag{11}$$

where, $A_C$and $T_C$are area and temperature of the condensing cover;h_{W-C} is the overall heat transfer coefficient between water and condenser and is equal to the sum of the convective ($h_{c,W-C}$), evaporative ($h_{e,W-C}$), and radiative ($h_{r,W-C}$) heat transfer coefficient. The h_{W-C} is obtained using

$$h_{W-C} = h_{c,W-C} + h_{e,W-C} + h_{r,W-C} \tag{12}$$

where [30],

$$h_{c,W-C} = 0.884\left((T_W - T_C) + \frac{(P_V(T_W) - P_V(T_C))(T_W + 273)}{269.8 \times 10^{-2} - P_V(T_W)}\right)^{\frac{1}{3}} \tag{13}$$

$$h_{e,W-C} = 16.273 \times 10^{-3}h_{c,W-C}\left(\frac{P_V(T_W) - P_V(T_C)}{T_W - T_C}\right) \tag{14}$$

$$h_{r,W-C} = \varepsilon_{eff}\sigma(T_W + 273)^2((T_W + 273) + (T_C + 273)) \tag{15}$$

In the above equations, σ and $\varepsilon_{eff}$are Stefan-Boltzmann coefficient and effective emissivity, respectively. $P_V(T_W)$ and $P_V(T_C)$ are saturation vapor pressure of water at the temperature of the basin water and saturation vapor pressure of water at the temperature of cover (condenser), respectively [18].

3.1.3. 3-1-3- Glass cover

Net energy reached to the glass cover, i.e. condensing cover (Plexiglas), is equal to the energy comes from the water minus the energy lost from the cover and fins to the ambient:

$$m_C c_{p,C}\frac{dT_C}{dt} = \dot{Q}_{W-C} - \dot{Q}_{r,C-sky} - \dot{Q}_{c,C-amb} - \dot{Q}_{f-amb} \tag{16}$$

where, m_C, $c_{p,C}$ are mass and specific heat of condensing cover (Plexiglas), respectively. $\dot{Q}_{c,C-amb}$ and $\dot{Q}_{c,f-amb}$ are the rate of

convective heat transfer from the cover and fins to ambient, respectively. $\dot{Q}_{r,C-sky}$ is the rate of energy lost from the cover to the sky (atmosphere) by radiative heat transfer. These heats losses are calculated using the following equations:

$$\dot{Q}_{r,\,C-amb} = A_C h_{r,C-sky}\left(T_C - T_{sky}^{eff}\right), \tag{17}$$

$\dot{Q}_{c,C-amb} = A_C h_{c,C-amb}(T_C - T_{amb})$, (18)where, $h_{r,C-sky}$ is the radiation heat transfer coefficient for heat transfer to the sky and $h_{c,C-amb}$ is the convection heat transfer coefficient for heat transfer to ambient, respectively. T_{sky}^{eff} is an effective sky temperature. The effective sky temperature is a function of many parameters including ambient temperature, relative humidity, time of the day, cloud coverage, and so on. Since no measured sky temperature values are available, for the Kerman city, effective sky temperature, T_{sky}^{eff} is estimated using the following equation:

$$T_{sky}^{eff} = \left(\frac{1}{2}T_{amb} + \frac{1}{2}T_{sky}\right) \tag{19}$$

where T_{sky} is clear sky temperature in Celsius degree and is obtained from Ref. [31]:

$$T_{sky} = 0.0552(T_{amb} + 273)^{1.5} - 273, \tag{20}$$

$h_{r,C-sky}$and $h_{c,C-amb}$are obtained from the following equations [28,30]:

$$h_{r,C-sky} = \varepsilon_C \sigma\left((T_C + 273)^2 + \left(T_{sky}^{eff} + 273\right)^2\right) \times \left((T_C + 273) + \left(T_{sky}^{eff} + 273\right)\right) \tag{21}$$

$$h_{c,C-amb} = \frac{k_{air}}{X_C} 0.59(Ra)^{0.25} \tag{22}$$

where, ε_C and X_C are the emissivity and the characteristic length of cover, respectively; Ra is Rayleigh number.

It is assumed that fins are all parallel and heat transfer from the fins to ambient is obtained using:

$$\dot{Q}_{f-amb} = A_f h_f (T_C - T_{amb}) \tag{23}$$

In the above equation, A_f is the effective area of the fins and h_f is convection heat transfer coefficient for fins, and it can be calculated from:

$$h_f = \frac{\left(Nu_f \times k_{air}\right)}{S} \tag{24}$$

Nu_f and S are Nusselt number and the average distance between steel plates used as fins, respectively. For natural convection heat transfer, Nusselt number is obtained as $Nu_f = 1.037$ [29].

3.1.4. 3-1-4-Distilled water yield and energy efficiency

In the numerical model, the freshwater production rate is obtained using the following equation:

$$\dot{m}_{dw} = \frac{h_{e,W-C} A_C (T_W - T_C)}{h_{fg}} \tag{25}$$

where, h_{fg} is the latent heat of vaporization of water. The hourly freshwater production rate is obtained by $\dot{m}_{dw,h} = \dot{m}_{dw} \times 3600$. Cumulative distilled water is the freshwater produced from the beginning to the current time and is obtained from $M_{dw,cum} = \int_0^t \dot{m}_{dw} dt$.

Total daily freshwater production is designated asM_{dw}.

Two energy efficiencies are defined in this study. The first one is the still efficiency which shows the performance of the still relative to the energy reached to the absorber. The daily still efficiency is defined as follows:

$$\eta_{still}^{E} = \frac{M_{dw} h_{fg}}{E_{Still}} \tag{26}$$

where $E_{still} = (\sum I_A(t) \times \delta t) A_A$ is solar energy reflected from the parabolic trough collector and hit the bottom of the solar still. δt is the time interval between two consecutive solar irradiance data.

The second efficiency is the system efficiency, η_{sys}^{E} , which shows the performance of the whole systems including parabolic trough collector and the solar still, relative to the energy reached to the aperture area of the collector. The daily system efficiency is calculated as

$$\eta_{sys}^{E} = \frac{M_{dw} h_{fg}}{E_{sys}} \tag{27}$$

where, $E_{sys} = A_{Ap} \times (\sum I_T(t) \times \delta t)$ and A_{Ap} is the aperture area of the parabolic trough collector. There is $A_{Ap} = CR \times A_A$ relation between aperture area and concentration ratio.

3.2. 3-2-Exergy analysis

3.2.1. 3-2-1-Absorber

Applying the exergy balance for the absorber and after some math, the following equation is obtained for the rate of exergy destruction in the absorber, $\dot{E}x_{des,A}$ [24,30]:

$$\dot{E}x_{des,A} = \dot{E}x_{sun} - \dot{E}x_{A-W} - \dot{E}x_{A-amb} - \dot{E}x_{stor,A} \tag{28}$$

where, $\dot{E}x_{sun}$, $\dot{E}x_{A-W}$, $\dot{E}x_{A-amb}$ and $\dot{E}x_{stor,A}$are the rate of exergy input from the sun to the absorber, the rate of exergy transfer from the absorber to the water (useful exergy), the rate of exergy dissipation from the absorber to ambient and rate of exergy change of the absorber, respectively. They are obtained from the following equations [32]:

$$\dot{E}x_{A-W} = \dot{Q}_{A-W}\left(1 - \frac{T_{amb} + 273}{T_W + 273}\right) \tag{29}$$

$$\dot{E}x_{A-amb} = \dot{Q}_{A-amb}\left(1 - \frac{T_{amb} + 273}{T_W + 273}\right) \tag{30}$$

$$\dot{E}x_{stor,A} = m_A c_{p,A} \frac{dT_A}{dt}\left(1 - \frac{T_{amb} + 273}{T_A + 273}\right) \tag{31}$$

$$\dot{E}x_{sun} = I_A A_A \left(1 - \frac{4}{3}\left(\frac{T_{amb} + 273}{T_{sun} + 273}\right) + \frac{1}{3}\left(\frac{T_{amb} + 273}{T_{sun} + 273}\right)^4\right) \tag{32}$$

where, T_{sun} is the effective blackbody temperature of the solar radiation reaches the earth.

3.2.2. 3-2-2-Saline water

Exergy is added to the water from the absorber and with the

inlet saline (brine) water. Part of input exergy is transferred from the saline water to the glass cover, some other is exited from the water by the outlet freshwater, another part is stored in the water, and the rest is dissipated. Furthermore, some exergy input to the water by the input brackish water and some exergy is lost by the distilled water discharge. The exergy transfer between saline water and the glass cover by evaporation is used to evaporate the water and can be called the useful exergy. The exergy balance equations for the saline water can be expressed as follows [24,30,32]:

$$\dot{E}x_{des,W} = \dot{E}x_{A-W} + \dot{E}x_{in} - \dot{E}x_{W-C} - \dot{E}x_{dw} - \dot{E}x_{stor,W} \tag{33}$$

where,

$$\dot{E}x_{in} = \dot{m}_{in}c_{p,W}\left((T_{in} - T_{amb}) - (T_{amb} + 273)\ln\left(\frac{T_{in} + 273}{T_{amb} + 273}\right)\right) \tag{34}$$

$$\dot{E}x_{W-C} = \dot{Q}_{W-C}\left(1 - \frac{T_{amb} + 273}{T_W + 273}\right) = h_{W-C}A_C(T_W - T_C)\left(1 - \frac{T_{amb} + 273}{T_W + 273}\right) \tag{35}$$

$$\dot{E}x_{dw} = \dot{m}_{dw}c_{p,W}\left((T_W - T_{amb}) - (T_{amb} + 273)\ln\left(\frac{T_W + 273}{T_{amb} + 273}\right)\right) \tag{36}$$

$$\dot{E}x_{stor,W} = m_W c_{p,W}\frac{dT_W}{dt}\left(1 - \frac{T_{amb} + 273}{T_W + 273}\right) \tag{37}$$

Exergy used for the evaporation of water, i.e. useful exergy, is obtained by

$$\dot{E}x_{e,W-C} = h_{e,W-C}A_C(T_W - T_C)\left(1 - \frac{T_{amb} + 273}{T_W + 273}\right) \tag{38}$$

3.2.3. 3-2-3-Glass cover

Some of the input exergy to the glass cover from the water is stored in the glass cover, some other is dissipated to ambient by convection and radiation heat transfer and the rest is dissipated in the cover. Applying the exergy balance for the glass cover gives the following equation [24,30,32]:

$$\dot{E}x_{des,C} = \dot{E}x_{W-C} - \dot{E}x_{C-amb} - \dot{E}x_{fin-amb} - \dot{E}x_{stor,C} \tag{39}$$

where,

$$\dot{E}x_{c,C-amb} = \dot{Q}_{c,C-amb}\left(1 - \frac{T_{amb} + 273}{T_C + 273}\right) \tag{40}$$

$$\dot{E}x_{r,C-amb} = \dot{Q}_{r,C-amb}\left(1 - \frac{4}{3}\left(\frac{T_{sky}^{eff} + 273}{T_C + 273}\right) + \frac{1}{3}\left(\frac{T_{sky}^{eff} + 273}{T_C + 273}\right)^4\right) \tag{41}$$

$$\dot{E}x_{fin-amb} = \dot{Q}_{fin-amb}\left(1 - \frac{T_{amb} + 273}{T_C + 273}\right) \tag{42}$$

$$\dot{E}x_{stor,C} = m_C c_{p,C}\frac{dT_C}{dt}\left(1 - \frac{T_{amb} + 273}{T_C + 273}\right) \tag{43}$$

3.2.4. 3-2-4-Exergy efficiency

Like energy efficiency, two exergy efficiencies are defined, i.e. still and system exergy efficiencies. The daily exergy efficiency of the solar still is obtained from:

$$\eta_{still}^{Ex} = \frac{Ex_{e,W-C}}{Ex_{sun}} \tag{44}$$

where, $Ex_{e,W-C} = \sum(\dot{E}x_{e,W-C} \times \delta t)$ and $Ex_{sun} = = \sum(\dot{E}x_{sun} \times \delta t)$.

The daily exergy efficiency of the solar still is defined as the following:

$$\eta_{sys}^{Ex} = \frac{Ex_{e,W-C}}{CR \times Ex_{sun}} \tag{45}$$

3.3. Numerical procedure

By writing energy balance for different parts of the new desalination system, a set of temperature-dependent equations are obtained. A computer program has been prepared for solving governing equations, i.e. Equations (1), (10) and (16) simultaneously. The governing equations are ordinary differential equations and each needs an initial condition. For the validation study, initial temperatures of different components of the still are taken equal to their corresponding initial temperature of experimental study. Otherwise, the initial temperature of absorber and water are assumed to be equal to ambient temperature, and the initial cover temperature is assumed to be equal to effective sky temperature. The above governing equations are solved iteratively using MATLAB built-in ode23tb differential equations solver. The exergy analysis is a post-process calculation and performs after energy equations are solved. The physical properties and operating parameters that are used in the thermal model are shown in Table 1.

4. Results

In what follows, numerical results obtained for the case that the parabolic trough collector is fixed with its slope is monthly adjusted at the optimal angle proposed by Jafari, and Javaran [27] is designated as *Fixed* and numerical results for the case that collector tracks the sun is designated as *Track*.

In the following, the density of water is assumed to be $1000kg/m^3 = 1kg/L$.

Table 1
Still parameters, physical [26] and thermophysical properties [32] used in the numerical simulation.

Property	Value	Property	Value	Property	Value
$m_A[kg]$	1.82	$k_W[W/(mK)]$	0.644	$C_{P,C}[J/(kgK)]$	1465
$C_{P,A}[J/(kgK)]$	500	$X_W = L_{bot}[m]$	0.05	$X_C[m]$	0.3
α	0.9	$k_P[W/(mK)]$	0.2	$S[m]$	0.02
$\tau_{g1} = \tau_{g1}$	0.9	$L_P[m]$	0.005	$h_{fg}[J/kg]$	2357E3
r	0.4	$k_{air}[W/(mK)]$	0.02551	ε_C	0.86
CR	6.4	$L_{air}[m]$	0.3	ε_W	0.95
$A_A[m^2]$	0.105	$m_C[kg]$	2.86	$T_{sun}[^0C]$	5504
$m_W[kg]$	2.381	$h_W[m]$	0.04		

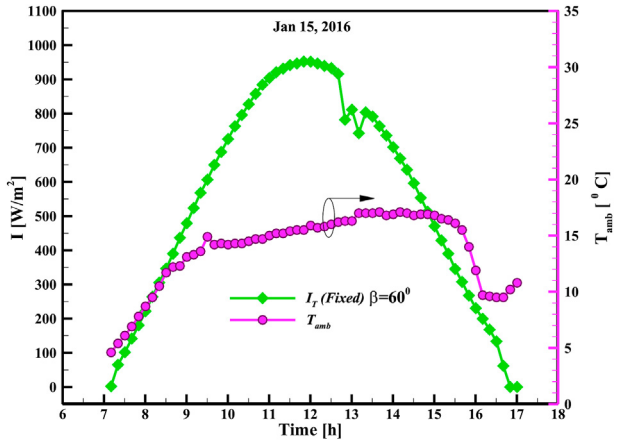

Fig. 2. Variation of solar irradiance and ambient temperature versus local time for the validation day (Jan 15, 2016).

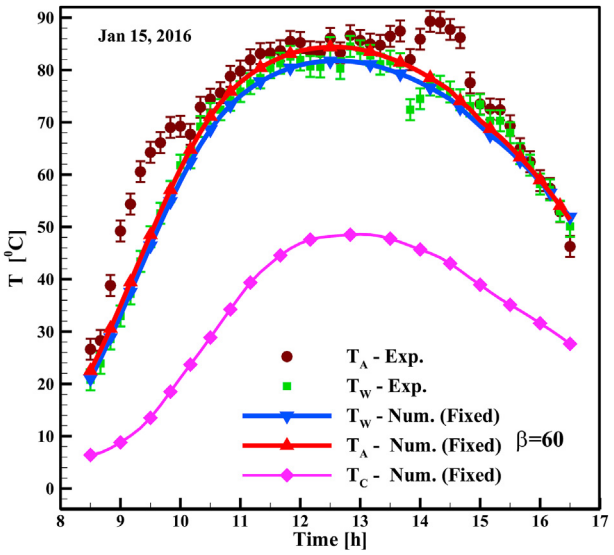

Fig. 3. Comparison of numerical (fixed collector slope) and experimental temperature of absorber and saline water for the validation day.

4.1. Model validation

Before using the thermal (numerical) model for the analysis of the new solar desalination system, it is validated by comparing its results with the experimental results [26]. The performance of the new solar still was experimentally tested in several days of Dec 2015 and Jan 2016. The thermal model is validated against these experimental results. However, to not repeat the same results several times, validation is just presented for Jan 15, 2016. In the following, a comparison between the results of the present model and experimental results obtained on Jan 15 is presented as a sample. The experiment was carried out from 8:30 a.m. to 4:30 p.m. Solar intensity over the ground and ambient temperature are taken from the Kerman meteorological office. Fig. 2 depicts the variation of solar irradiance over the aperture area of the collector (calculated using the isotropic sky model [28] and by using the ground solar irradiance provided by Kerman meteorological office [33]) and the ambient temperature (also provided by Kerman meteorological office) versus the local time for the day of the experiment. In this figure, $I_T(Fixed)$ is for the condition that the parabolic trough collector has fixed sloped ($\beta = 60^0$) like the experimental study.

All measurements, however careful and scientific, are subject to some uncertainties. The uncertainty is the possible difference between the measured and the real value of a parameter. Uncertainties may originate from the measuring instrument, from the measured item properties, from the environment, from the instrument operator, and from other sources. Uncertainties can be estimated using statistical analysis of a set of measurements and using other kinds of information about the measurement process. Uncertainty (accuracy) associated with the measuring instrument used in this study is presented in section 2. These uncertainties were obtained from the instrument datasheet or catalog. As mentioned above, the uncertainty of measured parameters, however, are not limited to the accuracy of instruments alone. The uncertainty analysis is performed to evaluate the overall uncertainty of the experimental measurements. The approach described by Taylor [34] is used to estimate the uncertainties in the experimental measurements. It is concluded that by considering all sources of uncertainty including user or operator uncertainty, the uncertainty of the temperature measurement and hourly distilled water yield with 95% confidence are ±1.5 °C and 15 mL, respectively.

In Fig. 3, the variation of the experimental and numerical absorber and water temperatures verses the local time are shown and compared for the validation day. As seen, there is a very good agreement between the temperatures obtained using the thermal model and the experimental temperatures. Fig. 4 shows a comparison between estimated and experimental accumulated freshwater production. As can be seen, the numerical and experimental results have the same trend and the present results have good agreement with the experimental one. The difference between the experimental and numerical results in the early hours of the experiment is might be partly because of solar energy reached and stored in the solar still components before starting the experiment.

In Table 2, a full day comparison between numerical results and experimental results is presented. The output and the performance of a solar still is directly related to the amount of solar radiation reaching on the absorber of solar still and to the ambient temperature. In this table, $\overline{T}_{amb}(^0C)$ is the average ambient temperature during the experiment; $M_{dw}(Lit)$ is total distilled water; $E_{sys}(MJ)$and

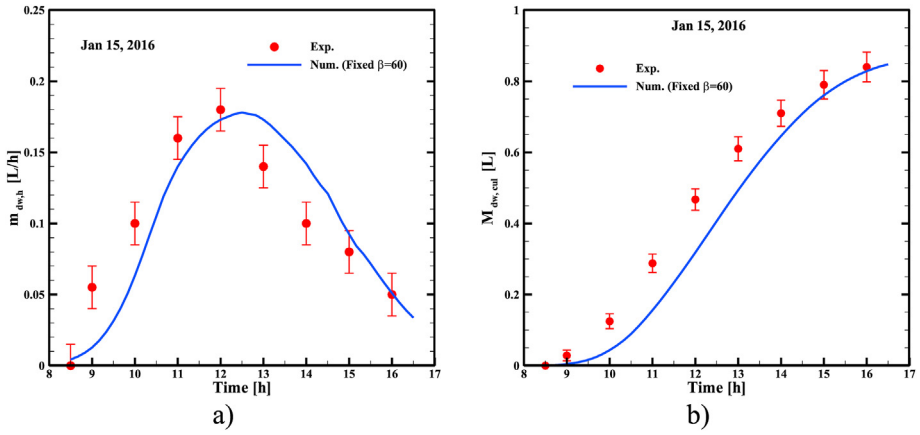

Fig. 4. Comparison of productivity obtained using the thermal model and experimental productivity for the validation day; a) hourly and b) accumulated freshwater production.

Table 2
Full day comparison of results obtained using the thermal model and experimental results at validating day (Jan 15, 2016).

	Status	Exp.	Num.
$\overline{T}_{amb}(^0C)$	–	16.3	16.3
$M_{dw}(L)$	*Fixed*	0.84	0.847
$E_{sys}(MJ)$	*Fixed*	6.27	6.27
$E_{still}(MJ)$	*Fixed*	–	3.60
$\eta^{E}_{sys}(\%)$	*Fixed*	14.75	14.77
$\eta^{E}_{Still}(\%)$	*Fixed*	–	55.74
$\eta^{Ex}_{sys}(\%)$	*Fixed*	–	5.58
$\eta^{Ex}_{Still}(\%)$	*Fixed*	–	9.64

$E_{still}(MJ)$ are total solar energy reaching the system (hit to the aperture of parabolic trough collector) and solar energy reaching the bottom of the still, respectively. All these parameters and averaging are calculated for the period of calculation or experiment.

As seen in Table 2, all quantities obtained using the thermal model have a very good agreement with the experimental results. Cooper [35] reported that the theoretical maximum energy efficiency of an ideal standard solar still is about 60%. The daily energy efficiencies of the new solar still (present study) are obtained numerically as 55.74% which is near to the maximum theoretical efficiency of standard solar still. The high efficiency of the solar still is due to the concentration of solar radiation that leads to the high temperature of the water in the basin. The exergy efficiency of the still and the new desalination system (i.e. solar still integrated into parabolic trough collector) are numerically calculated as 5.58% and 9.64%, respectively.

To check the performance of the present solar desalination system, its productivity is compared with a similar design. Concentrator-coupled hemispherical basin solar still with and without phase change materials (PCM) proposed and experimentally studied by Arunkumar et al. [36] to enhance productivity. Experimental results showed that the daily productivity of their desalination system with and without the PCM is 4.46 L/m^2/day (from 9 a.m. to 6:45 p.m.) and 3.52 L/m^2/day, respectively. With an absorber area of $A_A = 0.105m^2$, the productivity of the present system is $8.0L/m^2/day$. Comparison of the present new solar still composed of parabolic trough collector with built-in solar still with Arunkumar et al. [36] design shows that the present system has a good performance.

As mentioned in section 2, water and absorber temperatures were measured in the middle of basin water and at the center of the absorber respectively, while the temperatures obtained in the numerical model are average temperatures of the water and absorber. Some of the differences between the numerical and experimental temperatures might be because of the non-uniformity of temperature in the water and over the absorber in the experiment.

4.2. Effect of seasons

The performance of any solar still depends on the meteorological conditions especially solar radiation and ambient temperature. As these two parameters vary across the years (especially in different seasons), it is interesting to study the performance of the new solar still in different seasons of a year. In Iran like most of the world, a year is divided into four seasons including winter, spring, summer, and autumn. A variety of dates are used in different countries or regions to mark changes in the calendar seasons. In this study, it is assumed that spring begins on 1 March, summer on 1 June, autumn on 1 September, and winter on 1 December. Each season is represented by a single average day. A 10-min average daily (24 h) profile of ambient temperature and solar irradiation for each season is obtained by seasonal averaging of metrological data of the 2015 year (provided by the Kerman meteorological office) and is shown in Fig. 5. As the experimental data were collected only during the winter of 2016, in this section, only the simulation results will be presented. It can be observed that for most of the time the solar irradiance for the tracking parabolic trough collector ($I_T(Track)$) is higher than that of the identical fixed slope parabolic trough collector ($I_T(Fixed)$ at monthly optimal sloped angle proposed by Jafari and Javaran [27].

The variation of absorber temperature, water temperature and cover temperature of solar still for different seasons are shown in Figs. 6 and 7. It is seen that the temperatures of the absorber, water, and cover have the same trend as the solar irradiance with around half an hour delay (hint: Daylight saving time in Iran begins on March 20 or 21 and ends Sep 20 or 21 of each year). This temperature lagging is because of the heat capacity of the absorber, water, and cover. Also, from these figures, it can be noticed that in the case of solar tracking, the cover temperature, basin water temperature, and absorber temperature have a higher temperature than that of the fixed sloped collector. Finally, as shown in Figs. 6 and 7, the maximum reachable temperature would be slightly increased by increasing solar radiation and ambient temperature due to the nonlinear increase of heat loss to ambient at higher temperatures especially radiative heat transfer. The maximum absorber temperature happens in the summer season (around 90 °C) that has maximum solar irradiation and ambient temperature.

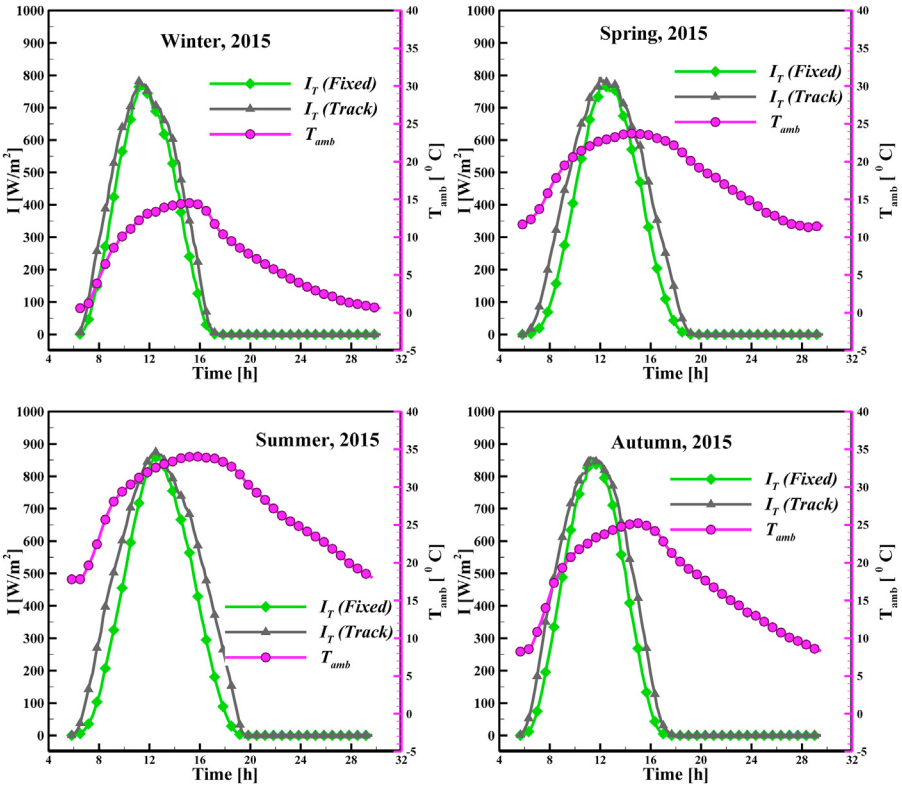

Fig. 5. Daily variation of ambient temperature and solar irradiance over the aperture area of parabolic trough collector for the average day of different seasons.

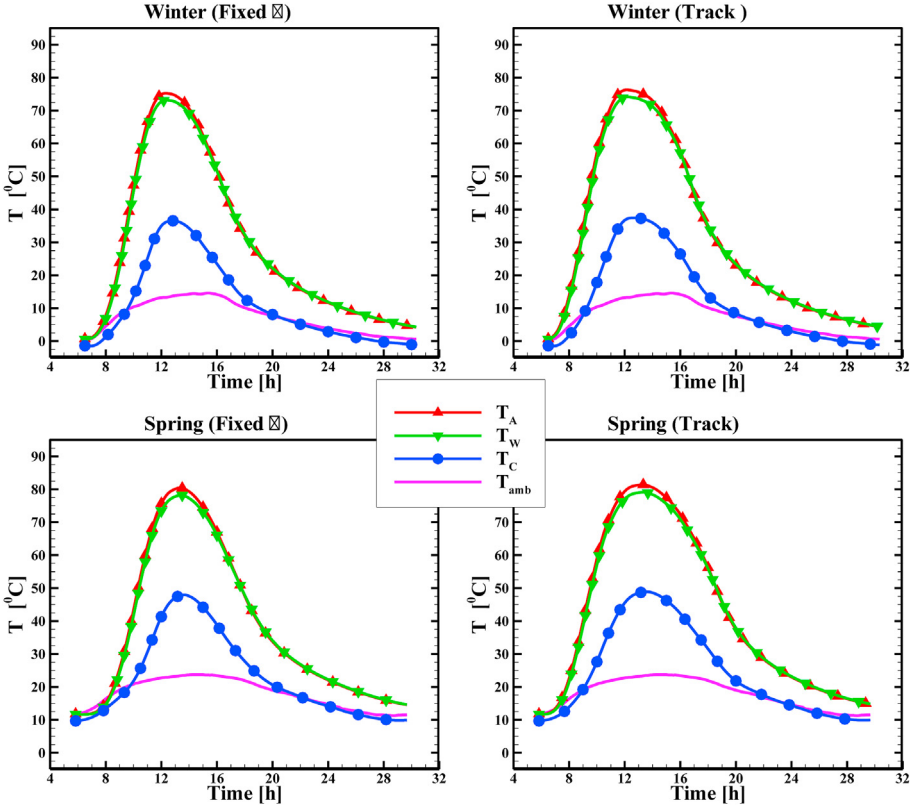

Fig. 6. Variation of the absorber, water, cover, and ambient temperature during average winter and spring days.

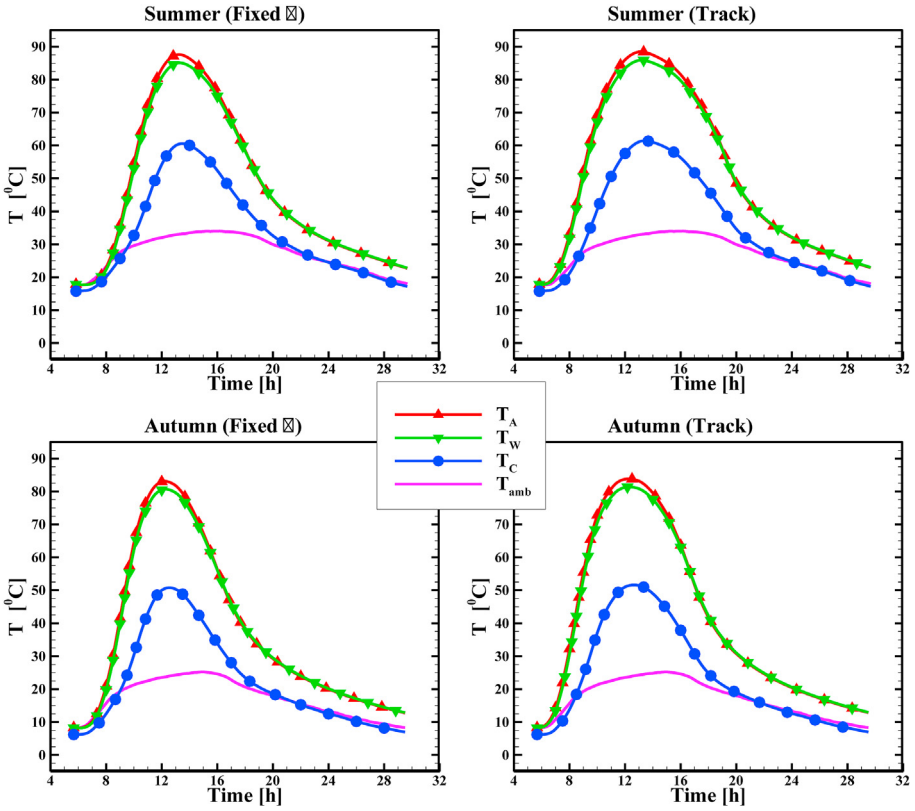

Fig. 7. Variation of the absorber, water, cover, and ambient temperature during average summer and autumn days.

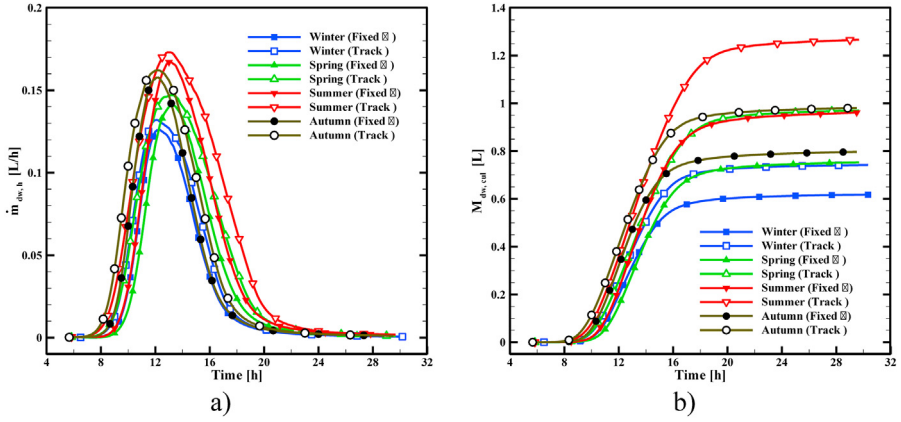

Fig. 8. a) The comparison of variation of freshwater productivity (rate) and b) the accumulative freshwater productivity for the average days of different seasons.

To reduce the number of figures and pages, from now on, results will be presented for winter and summer only. The hourly variation of freshwater productivity and accumulated freshwater yield with and without a tracking system for these two seasons are illustrated in Fig. 8. It is seen that the water productions are reached its maximum values around half an hour past the solar noon that is the time of maximum saline water temperature.

In Table 3, the average clock time of solar noon and average ambient temperature for each season, and whole-day performance of solar still at four seasons are presented. It can be observed from Fig. 8 and Table 3 that the freshwater productivity is greater when the tracking system is used. Also, using a tracking system increases the freshwater production by 20%, 29%, 32% and 23% for winter, spring, summer, and autumn, respectively. Furthermore, the highest and lowest freshwater production is summer and winter, respectively. The present solar still system produces 55% (70%) more freshwater in the average day of summer than the average day in winter for Fixed (Track) parabolic trough collector in Kerman weather conditions. Moreover, the new solar desalination system produces almost the same amount of freshwater in the average day of spring and autumn.

As Fig. 5 shows, both ambient temperature and solar irradiance are different at different seasons. Thus, both parameters affect the solar still performance. To separately study the effect of ambient temperature on the performance of solar still, a numerical experiment is performed to consider the effect of ambient temperature on

Table 3
Data and performance of the solar still integrated with the parabolic trough collector at average days of four seasons.

	Status	Winter	Spring	Summer	Autumn
$\overline{T}_{amb}(^0C)$	–	7.32	17.92	27.30	17.18
Ave. Solar noon	–	11:47	12:43	12:45	11:31
$\overline{I}_T(Wm^{-2})$	***Fixed***	174.4	189.68	222.33	198.32
	Track	202.98	237.99	282.60	238.92
$M_{dw}(L)$	***Fixed***	0.618	0.753	0.961	0.797
	Track	0.742	0.970	1.266	0.981
$E_{sys}(MJ)$	***Fixed***	5.03	5.47	6.41	5.72
	Track	5.85	6.86	8.15	6.89
$E_{still}(MJ)$	***Fixed***	2.89	3.16	3.66	3.28
	Track	3.37	3.97	4.72	3.96
$\eta^{E}_{sys}(\%)$	***Fixed***	13.42	15.04	16.39	15.23
	Track	13.85	15.45	16.99	15.56
$\eta^{E}_{Still}(\%)$	***Fixed***	50.34	56.18	61.92	57.20
	Track	51.78	57.64	63.25	58.39
$\eta^{Ex}_{sys}(\%)$	***Fixed***	4.56	4.58	4.60	4.76
	Track	4.88	4.91	4.99	5.05
$\eta^{Ex}_{Still}(\%)$	***Fixed***	7.90	7.97	8.00	8.28
	Track	8.40	8.48	8.48	8.76

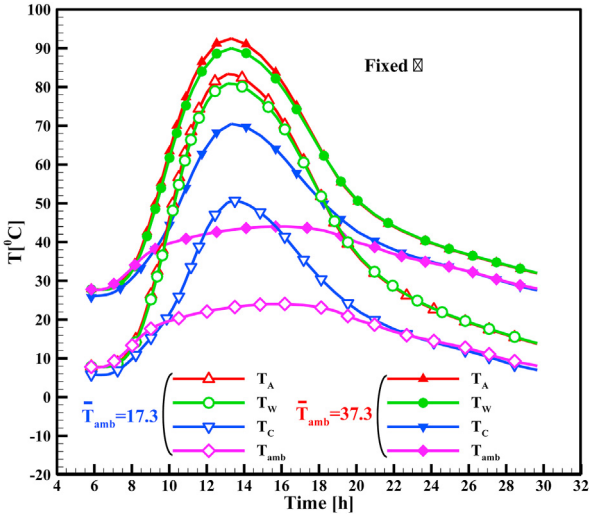

Fig. 9. Influence of ambient temperature on the variation of the absorber, water, and cover temperatures for the same solar radiation for the fixed collector.

productivity. For this experiment, all meteorological data is the same as the summer except ambient temperature and the parabolic collector is considered to not track the sun, i.e. fixed sloped parabolic trough collector. New ambient temperature, T^{New}_{amb}, is assumed to be equal to summer ambient temperature, T_{amb} (shown in Fig. 5), plus some fixed values, ΔT_{amb}, as follows:

$$T^{New}_{amb} = T_{amb} + \Delta T_{amb} \tag{46}$$

Four values are considered for ΔT_{amb}, i.e. −10 °C, −5 °C, 5 °C and 10 °C. The effect of these new ambient temperatures on productivity is shown in Table 4. As can be seen, there is a direct proportionality between the productivity of the solar still system and the ambient temperature. However, this relation is not linear especially at high ΔT_{amb}. For example, a 10 °C decrease in ambient temperature decreases productivity by 7.3%, and a 10 °C increase in ambient temperature increases productivity by 5.3%. By performing the same procedure for other seasons, the same trend in the relation between ambient temperature and productivity is observed. The experimental results of Rahbar et al. [37] are also shown the same trend. Present results show the importance of ambient temperature on productivity and revealed that productivity and efficiency are independently influenced by ambient temperature and solar energy. In other words, for meaningful performance comparison of solar stills, the energy and ambient temperature must be the same. Strictly speaking, a solar desalination system may have different productivity and efficiency for the same design and solar energy it received if the ambient temperature changes.

To study the effect of ambient temperature on the solar still performance in detail, two variations in ambient temperature i.e. $\Delta T_{amb} = -10$ and $\Delta T_{amb} = +10$ is selected to present results. Fig. 9 shows the effect of ambient temperature on the temperature of three components of the solar still, i.e. absorber, water, and glass cover. The effect of ambient temperature on the variation of convective, radiative, and evaporative heat transfer between water and cover is illustrated in Fig. 10. In this figure, heat transfer (loss) from the bottom surface and cover to ambient is also shown. As can be observed, for most of the time heat transfer from the cover to ambient is more than the one from the absorber to ambient. Also, the evaporative heat transfer dominates over the convective and radiative heat transfer from water to cover.

By considering Figs. 9 and 10, it is seen that if the ambient temperature is increased while the solar irradiance is kept constant, the absorber, water, and temperatures are all increased. However, the increase in cover temperature is more pronounced than others. Furthermore, the increase in ambient temperature would decrease the temperature difference between brackish water and cover and therefore decrease convective and radiative heat transfer between cover and water. However, as the evaporative heat transfer through the vapor pressure is exponentially related to water temperature despite the decrease in temperature difference, evaporative heat transfer between water and cover is increased (see Fig. 10). Also, from Fig. 10 b, it is found that the increase in the ambient temperature would increase heat transfer from cover to ambient that is due to the increase in evaporative heat transfer between water to cover.

The thermal losses from the solar still depend on the difference in the solar still temperature (absorber and cover), the ambient and the sky temperatures, and heat loss coefficients. As ambient temperature during the early morning of the day increased steadily and due to radiative heat transfer to the sky, the cover temperature is below ambient temperature and evaporative heat transfer between water and cover is almost zero and thus productivity is negligible in the early morning. Fig. 10 b) shows that in the early hour of the morning, heat transfer is negative and is from the atmosphere

Table 4
Effect of ambient temperature on the daily freshwater yield based on the summer data and for Fixed collector.

$\Delta T_{amb}(^0C)$	$\overline{T}_{amb}(^0C)$	$M_{dw}(L)$	$\Delta M_{dw}/M_{dw}(\%)$	$E_{sys}(MJ)$	$\eta^{E}_{sys}(\%)$	$\eta^{Ex}_{sys}(\%)$
−10	17.3	0.891	−7.3%	6.41	15.20	4.86
−5	22.3	0.932	−3.0%	6.41	15.89	4.77
0	27.3	0.961	–	6.41	16.39	4.60
5	32.3	0.997	3.8%	6.41	17.01	4.47
10	37.3	1.012	5.3%	6.41	17.26	4.23

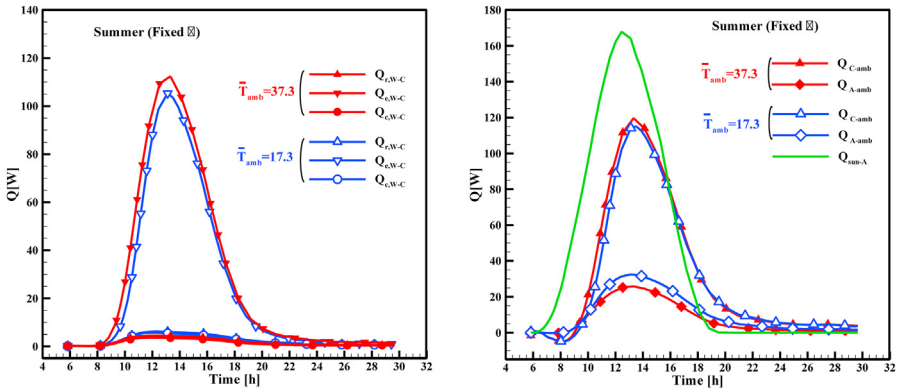

Fig. 10. Effect of ambient temperature a) on the evaporative, conductive, and radiative transfer between water and cover and b) on the heat transfer from the bottom and cover to ambient for the average summer day and for the fixed collector.

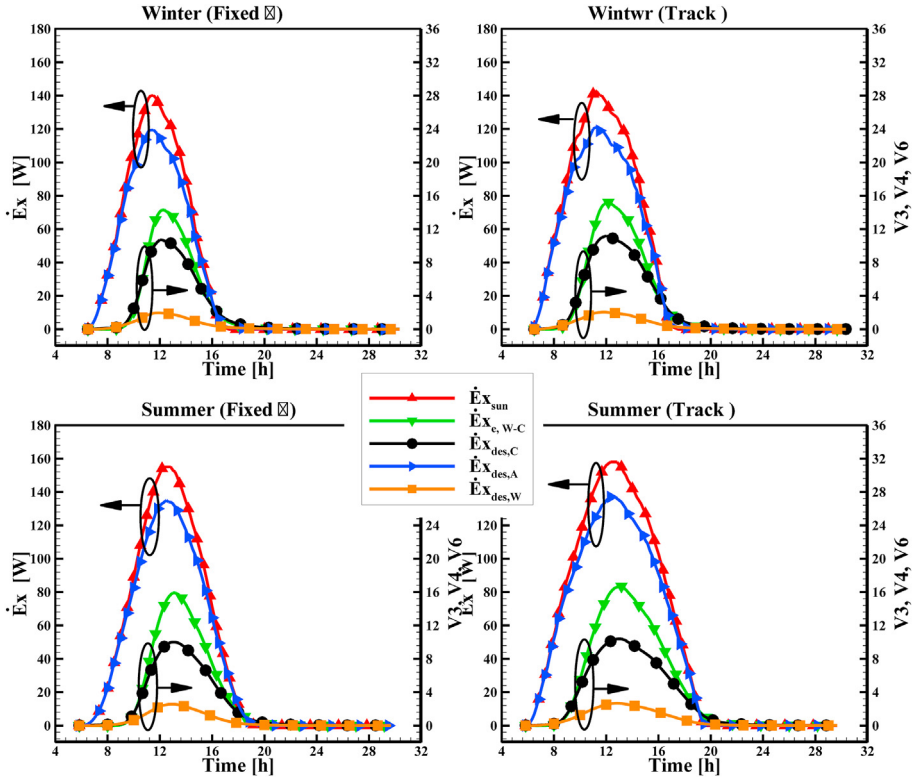

Fig. 11. Variation of solar exergy reached to the absorber, evaporative exergy transfer between water and cover and exergy destruction in the absorber, water and cover for average summer and winter days.

(ambient and sky) to the cover. For this hour, since absorber directly receives solar energy and due to low overall heat lost coefficient of the absorber, heat transfer from the atmosphere to the absorber (negative heat transfer) is small. Furthermore, Fig. 10b reveals that there is around half an hour delay between the maximum solar irradiance and maximum heat transfer from the absorber to ambient. The delay is around 1-h for heat transfer from cover to ambient. This is due to the storage of heat in the sensible form in the absorber, water, and cover glass. Due to this heat energy storage, after around 15:30 (3:30 p.m.) total heat transfer to ambient becomes more than solar energy reached to the absorber from the sun.

The rate of instantaneous solar exergy reached to the absorber, evaporative exergy transfer between water and cover, and exergy destruction in the absorber, water, and cover are presented in Fig. 11. For the other seasons, the trends are the same. These figures show that all exergies and exergy destruction are higher for the collector with the tracking system. Also, most of the exergy of the solar radiation is destructed in the absorber and only a small part of sun exergy is used for evaporation. Moreover, brackish water has the lowest exergy destruction among the three components of the soar still. This is due to the low-temperature difference between the absorber and saline water (see Figs. 6 and 7).

Table 3 shows that, in all seasons, the energy efficiency of still with the tracking system is higher than the still with fixed slope especially. It must be mentioned that the energy efficiency for the fixed and tracking system are calculated based on the energy received to each system. If energy efficiency defines based on

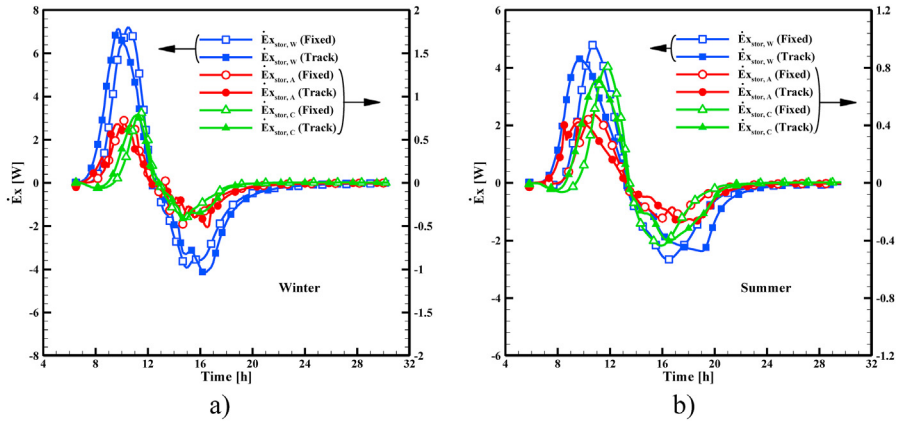

Fig. 12. Rate of change in the exergy stored in absorber, water, and cover for average summer and winter days.

energy received to the tracking system, the efficiency of the fixed system would be even lower than the current values. The difference between the efficiency of the two systems comes from the higher temperature of the water and other components of solar still with the tracking system. Like energy efficiency, the exergy efficiency of solar still with the tracking collector is higher than solar still with the fixed collector. At the absorber, the relatively high temperature of solar radiation (5777 K) is downgraded to the relatively low temperature (around 360 K) of the absorber. This leads to high exergy destruction in the absorber. Owing to the substantial destruction of energy quality at the absorber, for all the considered cases, the exergy efficiency is lower than the energy efficiency.

Fig. 12 shows the rate of change in exergy stored in the absorber, water, and cover for winter and summer. It can be seen in this figure that due to the higher heat capacity of water (mass of water multiplied by its specific heat capacity), the rate of change of exergy stored in water is higher than the absorber and cover. Furthermore, because of the continuous increase of solar irradiance in the morning, the rate of exergy storage is positive before noon. In the afternoon as the solar radiation decreases, energy stored is released and the rate of exergy storage becomes negative.

Tables 3 and 4 show that energy efficiency is directly related to ambient temperature and is higher in hotter seasons. In contrast, exergy efficiency is higher at colder seasons. Table 4 reveals that in contrast to energy efficiency, for the same irradiance during summer if the ambient temperature increases the exergy efficiency would be decreased. The reduction in the exergy efficiency is because of the reduction in temperature difference between absorber and ambient. The maximum temperature difference between absorber and ambient is around 50 °C for $\Delta T_{amb} = +10$ and is 60 °C for $\Delta T_{amb} = -10$ (see Fig. 9).

5. Conclusions

In this study, an unsteady thermal model is developed to numerically study a new standalone desalination system previously proposed and experimentally investigated by the authors. The new system is composed of a parabolic trough collector put under conventional solar still. The model is developed using the energy balance equations for different components of the system. The governing equations are solved numerically and validated using experimental data. The developed thermal model predicts the values of water and absorber temperature and yields with reasonable accuracy. With the help of the developed model, the performance and productivity of the solar still with a different design, climatic and operating conditions are predicted.

In the experimental study, the parabolic trough collector did not follow or track the sun. In the present work, the effect of using the tracker (active collector) for the parabolic trough collector on the performance of the new solar desalination system is evaluated numerically and compared with the regulated fixed sloped collector (passive collector). Results show that using the tracking collector can increase the productivity and performance of the desalination system especially in the early hour of the day and in the afternoon. Also, the performance of the new system is investigated at four seasons to consider the effect of climatic parameters.

The results of this study can be summarized as follows:

1 Comparison of the present solar desalination system, which is composed of parabolic trough collector with built-in solar still, with other similar designs shows that the present systems have a good performance.
2 The highest and lowest freshwater production is in summer and winter, respectively. In Kerman weather conditions, on average the present solar still system produces 55% more freshwater in summer than in winter for Fixed parabolic trough collector. For the parabolic trough collector with tracking systems, the system would produce 1.266 L per day in summer that is 70% more than winter.
3 The daily energy efficiency of the new solar desalination system and efficiency of the solar still can reach to 17% and 63%, respectively. These maximum efficiencies happen in summer.
4-For the same solar irradiation, energy efficiency, and freshwater production are higher at a higher temperature of ambient. For the same solar irradiation, the exergy efficiency is higher at colder ambient.
5 The absorber has the highest exergy destruction while brackish water has the lowest exergy destruction. Therefore, the selection of an appropriate absorber design plays an important role in the exergy improvement of solar stills.
6 Results show that energy efficiency in the summer and spring, that have a higher ambient temperature, is higher than autumn and winter.

It is shown that that within the different components of the solar still, the largest exergy destruction takes place in the absorber which is due to the high-temperature difference between the sun and the absorber. This means that current solar still designs have low exergy efficiency and there is plenty of room for improvement of these systems. To increase the exergy efficiency of solar stills, temperature over the absorber must be increased to near sun temperature. For this reason, solar still should be combined with

other solar systems. One way we think than can be used to reduce exergy destruction in solar stills is to employ solar concentrating systems with high concentration ratios to create high temperature over the absorber of a steam powerplant and then use the low-quality heat rejected from the powerplant for desalination. However, as known, a system with higher exergy efficiency does not necessarily mean that it is more energy-efficient and economically and practically possible.

CRediT authorship contribution statement

Hossein Amiri: Supervision, Writing - review & editing, Conceptualization, Methodology, Data curation. **Mohammad Aminy:** Conceptualization, Methodology, Data curation. **Marzieh Lotfi:** Data curation. **Behzad Jafarbeglo:** Data curation.

Declaration of competing interest

All authors have participated in (a) conception and design, or analysis and interpretation of the data; (b) drafting the article or revising it critically for important intellectual content; and (c) approval of the final version.

This manuscript has not been submitted to, nor is under review at, another journal or other publishing venue.

The authors have no affiliation with any organization with a direct or indirect financial interest in the subject matter discussed in the manuscript.

-Acknowledgement

The authors would like to acknowledge the financial support of the Institute of Science and High Technology and Environmental Sciences, Graduate University of Advanced Technology, Kerman, Iran, under grant number of 95/1839.

Nomenclature

$A[m^2]$	Area
$c_p[Jkg^{-1}K^{-1}]$	specific heat of the absorber
$CR\ [-]$	concentration ratio of the collector
$E\ [J]$	Total energy
$\dot{E}x[W]$	Rate of exergy transfer or destruction
$Gr\ [-]$	Grashof number
$I_A[Wm^{-2}]$	solar irradiance hitting the absorber
$I_T[Wm^{-2}]$	Solar irradiance over the aperture area
$h\ [Wm^{-2}K^{-1}]$	Convective heat transfer coefficient
$h_{fg}[Jkg^{-1}]$	the latent heat of vaporization of water
$k[Wm^{-1}K^{-1}]$	Thermal conductivity
$L\ [m]$	thickness
Nu	The Nusselt number
$m[kg]$	Mass
$\dot{m}\ [kgs^{-1}]$	Mass flow rate of water
$\dot{m}_{,h}[L/h]$	The hourly mass flow rate of water
$M_{dw,cum}([L],[kg])$	Cumulative distilled water
$P_V(T)\ [Pa]Pr\ [-]$	The Prandtl number
$\dot{Q}\ [W]$	Rate of heat transfer
$S\ [m]$	The average distance between fins
$r\ [-]$	Solar reflectivity of stainless steel
$t([s]\ or\ [h])$	Time
$T[^0C]$	Temperature
$U\ [Wm^{-2}K^{-1}]$	Overall heat transfer coefficient
$V_w\ [ms^{-1}]$	Wind speed
$X\ [m]$	Characteristic length

Greek

$\beta\ [rad]$	The slope of the collector
$\theta\ [rad]$	Angle of incidence
$\alpha\ [-]$	Solar absorption of the absorber
$\tau\ [-]$	Transmittance of the Plexiglas
$\varepsilon\ [-]$	emissivity
$\sigma\ [Wm^{-2}K^{-4}]$	the Stefan-Boltzmann constant
$\eta\ [-]$	efficiency
$\delta t\ [s]$	time interval

Subscripts

sys	system*amb*
C	cover
c	Convection*stor*
W	water*des*
A	Absorber
e	Evaporation
*g*1	Plexiglass layer 1
*g*2	Plexiglass layer 2
Ap	Aperture
iso	Isotropic sky model
P	Plexiglas
bot	Bottom
dw	Distilled water
in	Input
r	Radiative
eff	Effective
cum	Cumulative
f	Fin

Superscripts

eff	Effective
E	Energy
Ex	Exergy

References

[1] R. Sathyamurthy, T. Arunkumar, Different parameter and technique affecting the rate of evaporation on active solar still-a review, Heat Mass Tran. 54 (3) (2018) 593–630.
[2] T. Arunkumar, et al., A review of efficient high productivity solar stills, Renew. Sustain. Energy Rev. 101 (2019) 197–220, 2019/03/01/.
[3] G.M. Ayoub, L. Malaeb, Developments in solar still desalination systems: a critical review, Crit. Rev. Environ. Sci. Technol. 42 (19) (2012) 2078–2112.
[4] A. Muthu Manokar, K. Kalidasa Murugavel, G. Esakkimuthu, Different parameters affecting the rate of evaporation and condensation on passive solar still - a review, Renew. Sustain. Energy Rev. 38 (2014) 309–322.
[5] Z.M. Omara, A.S. Abdullah, A.E. Kabeel, F.A. Essa, The cooling techniques of the solar stills' glass covers – a review, Renew. Sustain. Energy Rev. 78 (2017) 176–193, 2017/10/01/.
[6] H. Panchal, D. Mevada, R. Sathyamurthy, The requirement of various methods to improve distillate output of solar still: a review, Int. J. Ambient Energy (2018) 1–7.
[7] K. Sampathkumar, T.V. Arjunan, P. Pitchandi, P. Senthilkumar, Active solar distillation-A detailed review, Renew. Sustain. Energy Rev. 14 (6) (2010) 1503–1526.
[8] V. Sivakumar, E. Ganapathy Sundaram, Improvement techniques of solar still efficiency: a review, Renew. Sustain. Energy Rev. 28 (2013) 246–264, 2013/12/01/.
[9] A. Somwanshi, A.K. Tiwari, Performance enhancement of a single basin solar still with flow of water from an air cooler on the cover, Desalination 352 (2014) 92–102, 2014/11/03/.
[10] R. Dev, S.A. Abdul-Wahab, G.N. Tiwari, Performance study of the inverted absorber solar still with water depth and total dissolved solid, Appl. Energy 88 (1) (2011) 252–264, 2011/01/01/.
[11] K. Selvaraj, A. Natarajan, Factors influencing the performance and productivity of solar stills - a review, Desalination 435 (2018) 181–187, 2018/06/01/.
[12] G.M. Zaki, A. Al-Turki, M. Al-Fatani, Experimental Investigation On Concentrator-assisted Solar-Stills, International Journal of Solar Energy 11 (3–4) (1992) 193–199, https://doi.org/10.1080/01425919208909739.
[13] H. Aburideh, A. Deliou, B. Abbad, F. Alaoui, D. Tassalit, Z. Tigrine, An experimental study of a solar still: application on the sea water desalination of Fouka, Procedia Eng. 33 (2012) 475–484.

[14] H. Hassan, M.S. Ahmed, M. Fathy, Experimental work on the effect of saline water medium on the performance of solar still with tracked parabolic trough collector (TPTC), Renew. Energy 135 (2019) 136–147.
[15] Z. Omara, A. Kabeel, M. Younes, Enhancing the stepped solar still performance using internal reflectors, Desalination 314 (2013) 67–72.
[16] H. Tanaka, Experimental study of a basin type solar still with internal and external reflectors in winter, Desalination 249 (1) (2009) 130–134.
[17] Z.M. Omara, A.E. Kabeel, M.M. Younes, Enhancing the stepped solar still performance using internal and external reflectors, Energy Convers. Manag. 78 (2014) 876–881, 2014/02/01/.
[18] G.N. Tiwari, S. Suneja, Performance evaluation of an inverted absorber solar still, Energy Convers. Manag. 39 (3–4) (1998) 173–180.
[19] B. Chaouchi, A. Zrelli, S. Gabsi, Desalination of brackish water by means of a parabolic solar concentrator, Desalination 217 (1–3) (2007) 118–126.
[20] S. Gorjian, B. Ghobadian, T. Tavakkoli Hashjin, A. Banakar, Experimental performance evaluation of a stand-alone point-focus parabolic solar still, Desalination 352 (2014) 1–17.
[21] R. Sathyamurthy, et al., A Review of integrating solar collectors to solar still, Renew. Sustain. Energy Rev. 77 (2017) 1069–1097, 2017/09/01/.
[22] T. Arunkumar, K. Vinothkumar, A. Ahsan, R. Jayaprakash, S. Kumar, Experimental study on various solar still designs, ISRN Renew. Energy 2012 (2012) 1–10, https://doi.org/10.5402/2012/569381.
[23] L. Malaeb, K. Aboughali, G.M. Ayoub, Modeling of a modified solar still system with enhanced productivity, Sol. Energy 125 (2016) 360–372.
[24] S. Sharshir, A. Elsheikh, G. Peng, N. Yang, M. El-Samadony, A. Kabeel, Thermal performance and exergy analysis of solar stills–A review, Renew. Sustain. Energy Rev. 73 (2017) 521–544.
[25] A. Kianifar, S. Zeinali Heris, O. Mahian, Exergy and economic analysis of a pyramid-shaped solar water purification system: active and passive cases, Energy 38 (1) (2012/02/01/2012) 31–36.
[26] H. Amiri, M. Lotfi, M. Aminy, B. Jafarbeglo, Design, fabrication and modeling of a new solar still desalination system and evaluation of its performance, J. Solid Fluid Mech. 8 (2) (2018) 205–220.
[27] S. Jafari, E.J. Javaran, An optimum slope angle for solar collector systems in kerman using a new model for diffuse solar radiation, Energy Sources, Part A Recovery, Util. Environ. Eff. 34 (9) (2012) 799–809.
[28] J.A. Duffie, W.A. Beckman, Solar Engineering of Thermal Processes, John Wiley & Sons, 2013.
[29] Y.A. Cengel, Heat Transfer: A Practical Approach, second ed. ed., McGraw-Hill, New York, 2002.
[30] S. Vaithilingam, G.S. Esakkimuthu, W. Treatment, Energy and exergy analysis of single slope passive solar still: an experimental investigation, Desalination 55 (6) (2015) 1433–1444.
[31] W.C. Swinbank, Long-wave radiation from clear skies, Q. J. R. Meteorol. Soc. 89 (381) (1963) 339–348.
[32] Y.A. Çengel, M.A. Boles, Thermodynamics: an Engineering Approach, McGraw-Hill, 2002.
[33] Kerman meteorological office, Available: http://kerman-met.ir/.
[34] J. Taylor, Introduction to Error Analysis, the Study of Uncertainties in Physical Measurements, 1997.
[35] P. Cooper, The maximum efficiency of single-effect solar stills, Sol. Energy 15 (3) (1973) 205–217.
[36] T. Arunkumar, D. Denkenberger, A. Ahsan, R. Jayaprakash, The augmentation of distillate yield by using concentrator coupled solar still with phase change material, Desalination 314 (2013) 189–192, 2013/04/02/.
[37] N. Rahbar, A. Asadi, E. Fotouhi-Bafghi, Performance evaluation of two solar stills of different geometries: tubular versus triangular: experimental study, numerical simulation, and second law analysis, Desalination 443 (2018) 44–55.